3

ZnO Nanorods: Synthesis by Catalyst-Free CVD and Thermal Growth from Salt Composites and Application to Nanodevices

Oleg V. Kononenko[1], Arkady N. Redkin[1], Andrey N. Baranov[3], Gennady N. Panin[1,2], Artem A. Kovalenko[4] and Anatoly A. Firsov[1]
[1]*Institute of Microelectronics Technology and High Purity Materials, RAS Chernogolovka, Moscow region,*
[2]*Quantum-Functional Semiconductor Research Center, Department of Physics, Dongguk University, Seoul,*
[3]*Chemistry Department, Moscow State University Moscow,*
[4]*Department of Materials Science, Moscow State University, Moscow,*
[1,3,4]*Russia*
[2]*South Korea*

1. Introduction

Zinc oxide (ZnO) is a unique functional semiconductor material with a wide band gap (3.37 eV), high binding energy of the exciton (60 meV) at room temperature, and an effective ultraviolet luminescence (Özgür et al., 2005). Materials based on ZnO can be used as chemical (Fan & Lu, 2005) and biological (Yang et al., 2009, Yeh et al., 2009) sensors, solar cells (Law et al., 2005, Wei et al., 2010), light emitting diodes (Park & Yi, 2004), laser (Huang et al., 2001, Govender et al., 2002), and composite materials (Hu et al., 2003). Zinc oxide is a biocompatible material with antiseptic properties. Quasi one-dimensional (1D) structures on the basis of zinc oxide are a promising material for nanoelectronics (Park et al., 2005).

In recent years, there has been an increasing interest in quasi one-dimensional nanocrystalline zinc oxide (nanorods, nanowires, and nanowhiskers), motivated by its perfect crystal structure and unusual properties due to size effects. In addition, single-crystal samples make it possible not only to raise the exciton density and create low-threshold gain media but also to reduce scattering losses. In this context, aligned arrays of single-crystal nanorods 20–200 nm in diameter and several microns in length are of special interest. Currently the optical properties of ZnO as a semiconductor material with good luminescent properties are of greatest interest. This is due to the possibility of applying materials on the basis of zinc oxide in the creation of new effective optoelectronic devices.

An effective approach for creation of nanodevices for light emitting and field emission is fabrication of vertically aligned ZnO 1D structures. Aligned ZnO nanocrystal arrays on substrates are commonly grown using thin metal film as a catalyst for 1D growth and different methods, such as vapor-liquid-solid (VLS) process (Zhao et al., 2003), metal-

organic chemical vapor deposition (MOCVD) (Park & Yi, 2004) or sol-gel process (Krumeich et al., 1999). The drawback to this method is that the nanocrystals may be contaminated with the catalyst (Collins et al., 1957 and Oh et al 2008). Moreover, catalyst particles as a rule remain on the tips of the grown zinc oxide nanocrystals (Kim et al., 2005 and J. Park et al., 2003). Catalyst-Free Chemical Vapor Deposition (CVD) is a promising method for ZnO nanostructure synthesis of high structural and optical perfection. Up to now, few papers have been devoted on the subject of catalyst-free growth of ZnO nanowire and nanorod arrays at temperature below 600°C (W.I. Park et al., 2003; Umar et al., 2005; Liu et al., 2005; Wang et al., 2005).

It is well known that the dopants can control the electronic and luminescence properties of the material. In recent years, attention has also focused on spin-dependent phenomena in dilute magnetic zinc oxide in which stoichiometric fraction of the zinc atoms are replaced by transition metal atoms. The growth from the salt mixture is promising method for doping of ZnO nanorods by transition metals and acceptor dopants.

2. Catalyst-free CVD synthesis of ZnO nanorods

The growth of ZnO nanorods was carried out by the elemental vapor-phase synthesis at a reduced pressure in flow-type reactor, developed earlier (Red'kin et al., 2007). A high-purity metallic granulated zinc (99.99%) was placed in an alumina boat which was then inserted at the end of quartz ampoule sealed at one end. At the open end, the ampoule had a wide slit, below which substrates were mounted with their front sides up. The ampoule was introduced into a horizontal two-zone flow-type quartz reactor so that the zinc source was located in one of the zones (evaporation zone), and the substrates, in the other (growth zone).

The reactor was first evacuated with forevacuum pump for 1 h and then high-purity argon (99.999%) was introduced into the reactor without terminating of evacuation. As a result, the steady-state pressure in the reactor reached 10^3 Pa. Then the temperature in the growth zone (t_2) was raised to the working one, 500 – 550 °C. Next, the temperature in the evaporation zone (t_1) was raised to reach 610 – 620 °C, and then high-purity oxygen (99.999%) was introduced into the reactor. The total flow of argon–oxygen mixture was 66.7 sccm. The oxygen concentration in the mixture was 10 vol. %.

During the process zinc vapor from the evaporation zone reached the growth zone and reacted with oxygen. Zinc vapor flow was 10 – 12 g/h. Under the above conditions, zinc/oxygen molar ratio in the vapor phase was about 5/1. The synthesis time was 30 - 40 min.

The growth of arrays of ZnO well aligned nanorods is very sensitive to synthesis parameters. In earlier works we made an extensive study in order to determine the regularities and optimum conditions for elemental vapor synthesis of highly aligned ZnO nanorod arrays on (100) and (111) silicon and glass substrates (Red'kin et al., 2007, 2009). Note also, that neither 1D growth catalyst nor zinc oxide buffer layers were deposited preliminary onto the substrates. The vertical growth of nanorods was observed on single-crystalline substrates and on amorphous glass substrates, which indicates that a substrate crystallography exerts no appreciable effect on nanorod growth direction under the conditions of these experiments.

Electron microscopy examination of the samples showed that ZnO nanorods normally directed towards a substrate surface grew on all the substrates used. The degree of array misalignment primarily depends on their position in the growth zone. In the first part of the growth zone located closer to the zinc vapor source, arrays of nanorods are uniform in size and mainly directed normal to the substrate surface irrespective of a substrate type.

As a rule, nanorods with the most uniform vertical alignment grow at the beginning and in the middle of the growth zone. A more detail analysis of the arrays revealed a relationship between the density of nanorod positioning on a substrate and the degree of their ordering. In more ordered arrays on Si (100) and Si (111) the density of nanorods is by 20 – 25% higher than in less ordered arrays on substrates of the same type. Arrays of approximately equal density on various substrates have similar distribution of nanorod growth directions. As have shown rocking curves the deviation from the normal direction of growth in these samples do not differ very much. So, the density of ZnO nanocrystals per square unit on a substrate is one of the factors which determine the uniformity of nanorod direction distribution in an array. Nanorod diameter also plays a certain role. It was noted that arrays of thicker nanorods are more uniformly vertically aligned. In other words, the more closely packed the growing nanorods, the more uniform is their vertical growth.

Note that initial stages of ZnO nanocrystals nucleation are of important role. Earlier we supposed that the growth of ZnO nanorods proceeds by VLS process under the conditions of our experiment. In the initial step nanodrops of metal zinc condensed on the substrate surface because of the temperature difference in the evaporation and growth zones. Further they act as a 1D growth catalyst (Red'kin et al., 2009). This "self-catalysis", with metal zinc droplets acting as catalyst of 1D growth of ZnO nanocrystals, was also described elsewhere (Wei et al., 2005; Zha et al., 2008). According to this mechanism, the initial density of zinc nanodrops on a substrate determines the nanorod density in a grown array. It explains why the uniformity of vertical growth is, as a rule, higher in the part of the growth zone which is closer to the zinc evaporation zone. The relationship of ZnO nanorods density and thickness and uniformity of vertical nanorod growth was observed earlier (Reiser et al., 2007, Zhao et al., 2005, Lee et al., 2007), where a similar conclusion was made concerning the effect of nucleation density on predominant direction of ZnO nanocrystal growth and uniformity of arrays grown by different methods.

Another difference of the self-catalysis from Au catalyst growth is that the diameter of catalyst droplets can both to decrease, and to increase, depending on relationship of zinc and oxygen partial pressure. It allows us to control nanorod shape by varying growth parameters such as zinc source and substrate temperature, reactor pressure and oxygen concentration. Figures 1-5 shows various types of nanorod morphology, which can be obtained by changing growth parameters during nanorod synthesis. Diameter of nanorods can decrease (fig.1, 2) or increase (fig.3) or it can alternately occur (fig.4). If change Zn partial pressure occurs suddenly rather big Zn drops can break up to the small ones. It leads to that on the tip of nanorods several nanorods with smaller diameters start to grow (fig.5).

To estimate the crystal perfection of nanorods in the grown samples, we studied their cathode-luminescence (CL) spectra. CL spectra were measured in two modes: direct and panchromatic, which allowed a comparison of the emission areas and the electron microscopy image of the nanorods on the substrate. As is seen from fig.6, the measured emission was mainly from the top faces of ZnO nanorods. The CL spectra showed that the

grown nanorods were of high quality, irrespective of the substrate type. The spectra of all samples (fig.7) contain only one strong UV band of the edge emission peaking at 382 nm due to free exciton recombination and no green and blue lines which are usually attributed to point defects in ZnO, such oxygen and zinc vacancies (Gruzintsev & Yakimov, 2005).

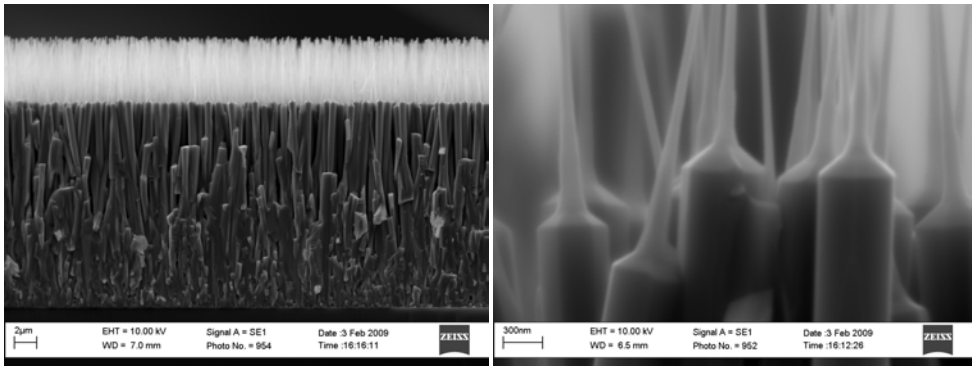

Fig. 1. (Left) scanning electron microscope (SEM) image of the cross-section of the ZnO nanorods arrays grown on Si (100) substrate. In the end of synthesis partial pressure of zinc was decreased. (Right) magnified SEM image of the ZnO nanorods shown in the left photo.

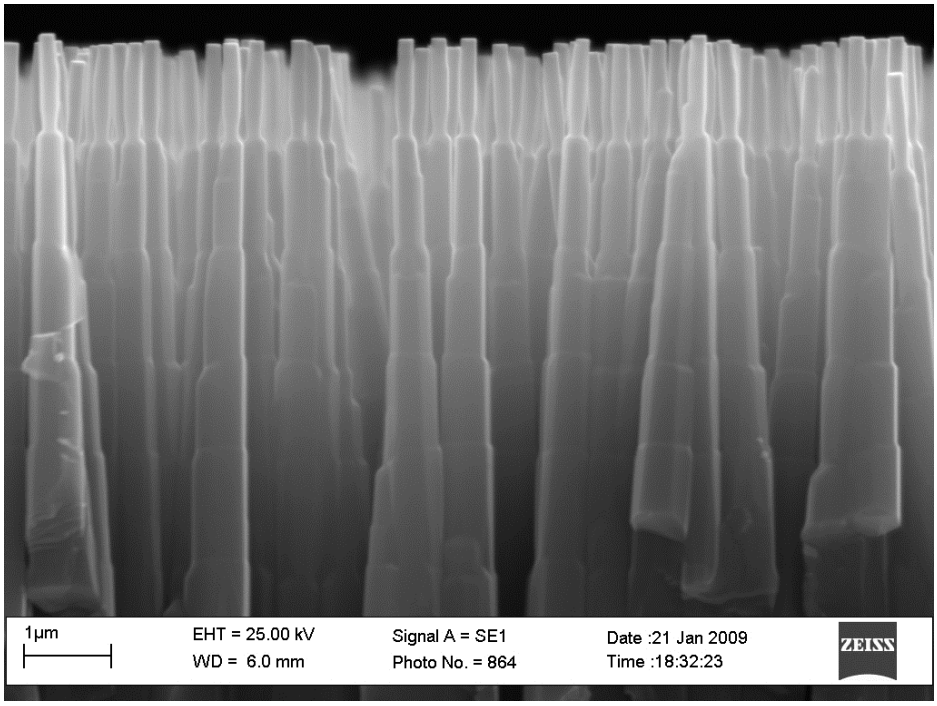

Fig. 2. SEM image of the cross-section of the ZnO nanorods arrays grown on Si (100) substrate. During synthesis zinc partial pressure was lowered in equal intervals.

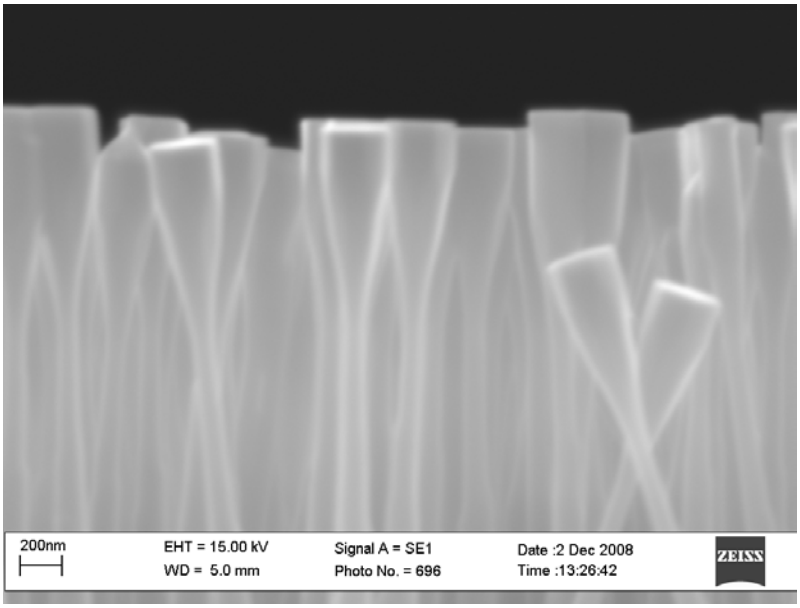

Fig. 3. SEM image of the cross-section of the ZnO nanorods arrays grown on Si (100) substrate. A partial pressure of oxigen was decreased near the end of synthesis.

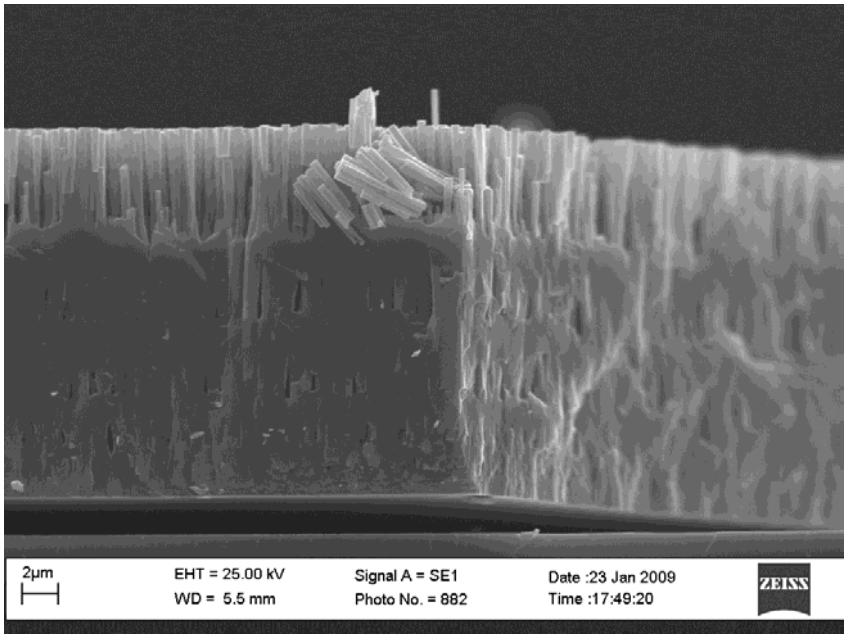

Fig. 4. SEM image of the cross-section of the ZnO nanorods arrays grown on Si (100) substrate. During synthesis zinc partial pressure was lowered and raised alternately.

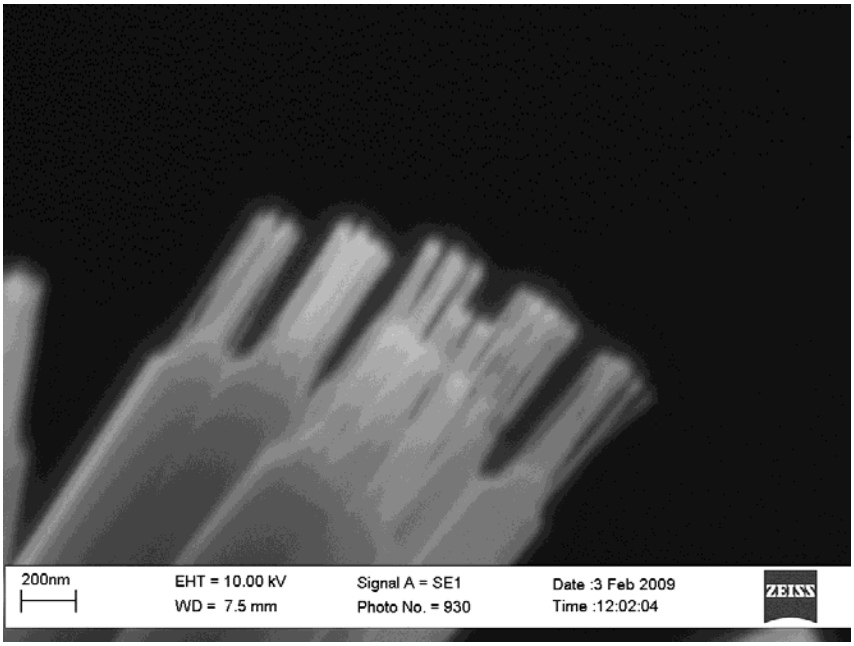

Fig. 5. SEM image of the cross-section of the ZnO nanorods arrays grown on Si (100) substrate. In the end of synthesis partial pressure of zinc was sharply lowered.

3. ZnO nanorod p-n homojunction

Stable and reproducible p-type ZnO for fabricating ZnO homojunction optoelectronic devices still remains challenging (Look et al., 2004).

ZnO single crystals and epitaxial films contain, as a rule, quite a few of intrinsic defects (usually higher than 10^{16} cm^{-3}). Majority of intrinsic defects are donors. When ZnO is doped with an acceptor, the compensation of donors takes place. The inversion of the n-type conductivity into the p-type one is possible only in samples with a low initial concentration of intrinsic defects under conditions when the compensation of the acceptors by the donor defects is minimized.

Sb was deposited by thermal evaporation onto the tops of aligned ZnO nanorod arrays grown by the catalyst-free elemental vapor-phase synthesis on n^+-Si(100) substrats. Then samples were annealed at 420°C in air atmosphere during different time.

CL spectrometry was used to measure the optical properties of Sb-doped ZnO nanorods (fig.8-10). For short-time annealed samples, a peak at 370.5 nm is dominant, which may be associated with donor-bound exciton emissions (fig.8). A peak at 380.3 nm may be associated with Sb-dopant. For medium-time annealed samples, both peaks are about of the same intensity (fig.9). For long-time annealed samples, a peak at 377.7 nm becomes dominant (fig.10). The peak positions are shifted to lower energies due to effects arising from the increased Sb-dopant concentration.

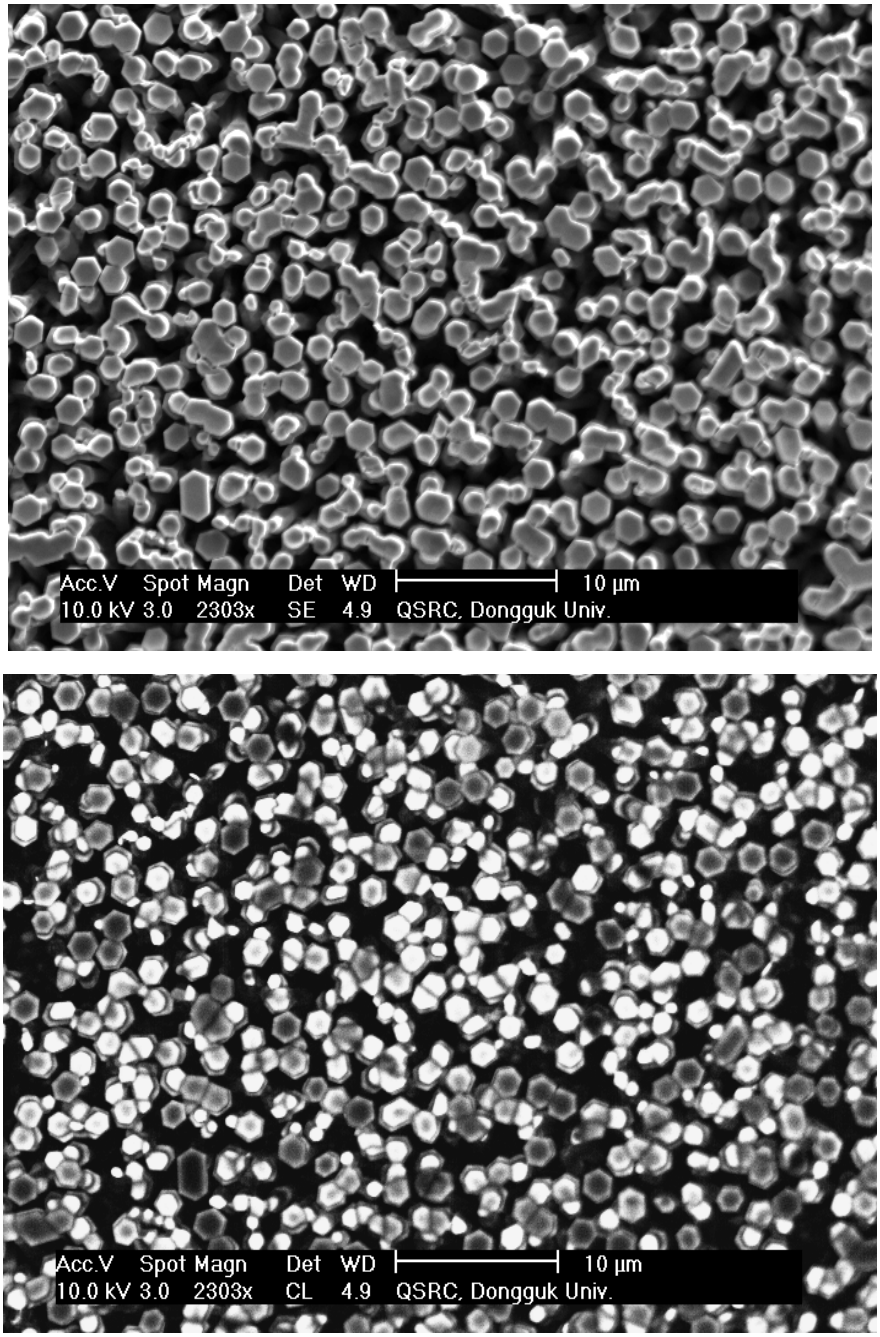

Fig. 6. SEM (top) and CL (bottom) images of a ZnO nanorod array grown by the elemental vapor-phase synthesis.

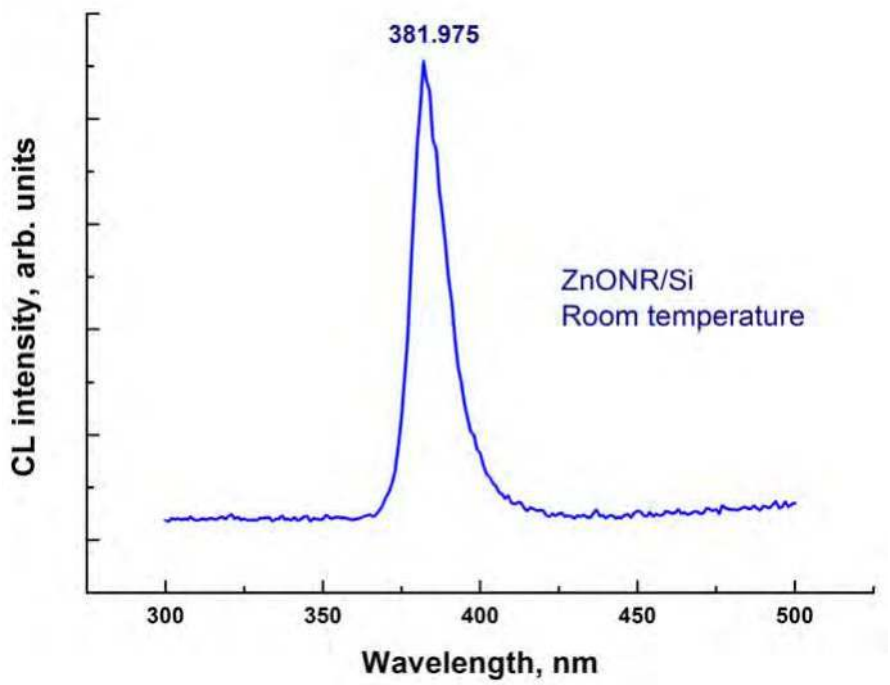

Fig. 7. CL spectrum of a ZnO nanorod array grown by the elemental vapor-phase synthesis.

Electrical contacts were prepared to Sb-doped ZnO nanorods and to n^+-Si (100) substrate. *I-V* characteristics were measured for all three samples. However, *I-V* curve only of the long-time annealed sample shows good rectification (fig.11). Blue light could be seen clearly from the diode by the naked eye (fig.12). The emission has been detected at ~6 V and increases with increasing the bias voltage (Kononenko et al., 2009).

4. ZnO nanorod p-n heterojunction

As the inversion of n-type conductivity to p-type conductivity in ZnO is a challenge so far, the other p-type wide band gap semiconductors and organic materials can be used for p-n junction fabrication on the basis of ZnO materials. Such semiconductors those are compatible with zinc oxide are $SrCu_2O_2$, $CuAlO_2$, GaN and NiO (Ohta & Hosono, 2004). The fabrication of hybrid heterojunction diodes have been reported in several works (Park & Yi, 2004, Zhang et al., 2009). These materials however require complex deposition techniques, such as the Molecular Beam Epitaxy, Chemical Vapor Deposition, Pulsed Laser Deposition. NiO and organic materials are an exception to this range. NiO can be synthesized by the thermal vacuum evaporation at the oxygen pressure of the order of 10^{-4}–10^{-5} Torr. In addition, a high enough (on the order of 10^{19} - 10^{20} cm^{-3}) hole concentration in the NiO films can be obtained. Organic materials can be deposited on ZnO materials by the spin coating. The fabrication of an inorganic/organic heterostructure diodes have been reported in references (Konenkamp et al., 2004, Konenkamp et al., 2005, Sun et al., 2008).

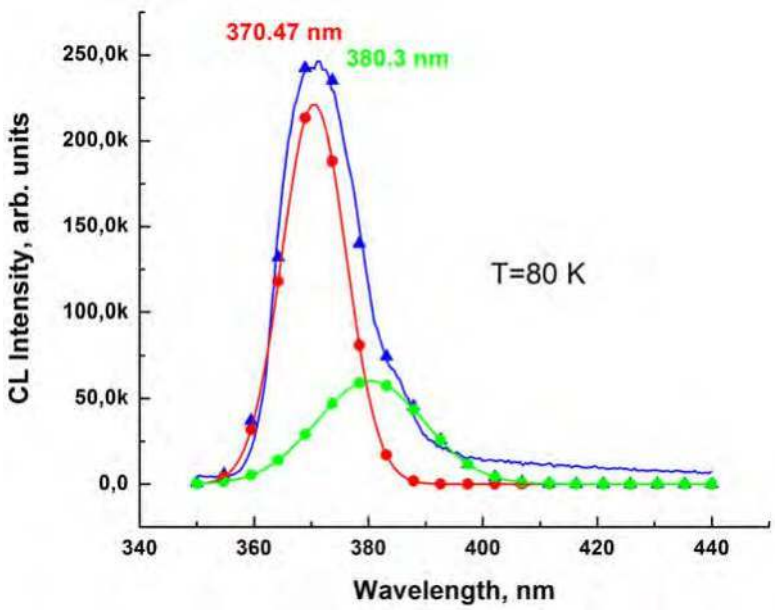

Fig. 8. CL spectrum of short-time annealed Sb-doped ZnO nanorod arrays grown on n^+-Si (100) substrate.

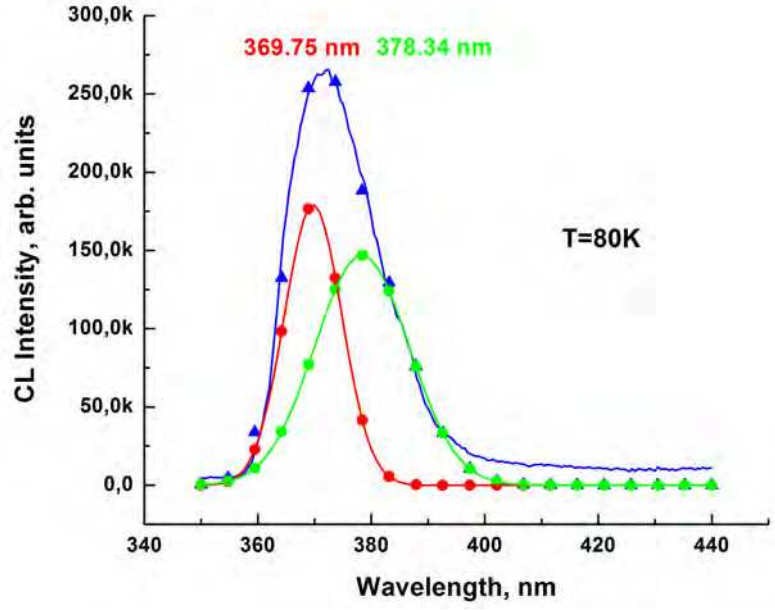

Fig. 9. CL spectrum of medium-time annealed Sb-doped ZnO nanorod arrays grown on n^+-Si (100) substrate.

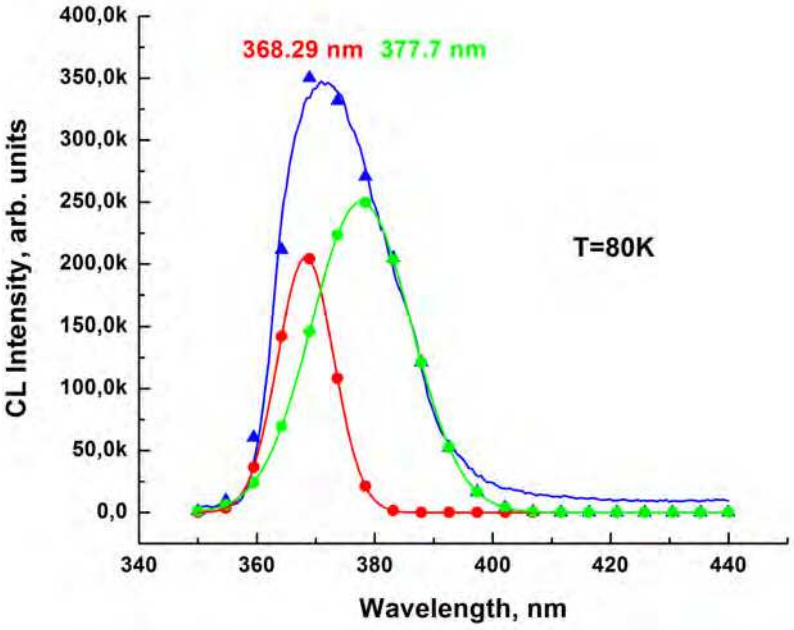

Fig. 10. CL spectrum of long-time annealed Sb-doped ZnO nanorod arrays grown on n^+-Si (100) substrate.

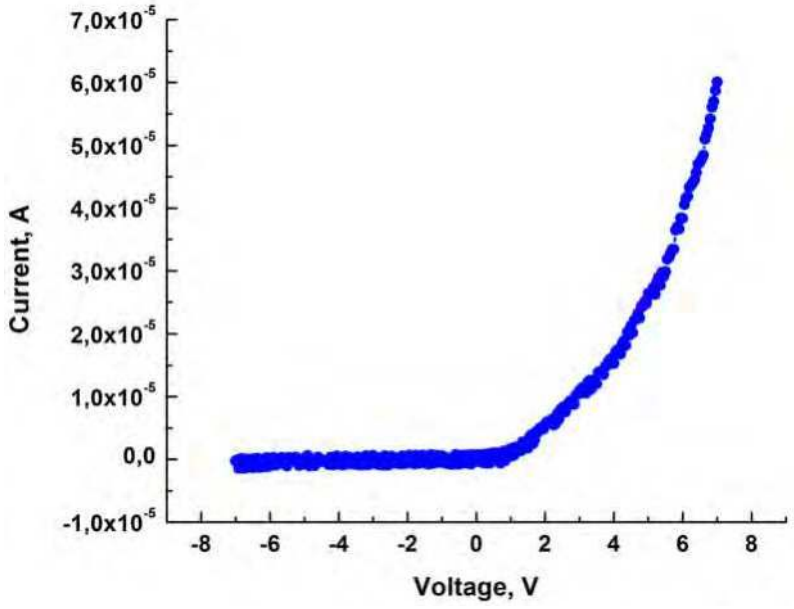

Fig. 11. The current-voltage characteristics of the Sb-doped ZnO nanorods diode.

Fig. 12. The optical micrograph of blue emission from the Sb-doped ZnO nanorods diode.

Two types of vertical structures were fabricated on the basis of ZnO and NiO. NiO film was deposited by e-beam evaporation of high purity Ni in an oxygen atmosphere at a partial pressure of 10^{-5} Torr on Si (100) substrate. Vertically aligned ZnO nanorods were grown by the catalyst-free elemental vapor-phase synthesis on the NiO film. Indium electrodes were prepared on the top of nanorods and the NiO film. The other structure was fabricated as follows. Vertically aligned ZnO nanorods were grown on Si (100) substrate. Then NiO was deposited by e-beam evaporation of high purity Ni in an oxygen atmosphere at a partial pressure of 10^{-5} Torr. Ni electrode was deposited in vacuum onto NiO and indium electrode was deposited on ZnO.

An inorganic-organic hybrid heterostructure was fabricated as follows. Vertically aligned ZnO nanorods were grown on indium tin oxide (ITO) glass substrate. Poly(methyl methacrylate) (PMMA) was spin-coated on the grown nanorods to provide a smooth surface for subsequent thin film deposition. A drop of poly(3,4-ethylene-dioxythiophene) (PEDOT)/ polystyrenesulfonate(PSS) was spin coated on the top of ZnO nanorods at a spin speed of 2000 rpm. Finally, a copper wire was attached on the surface of the PEDOT/PSS film using silver paste as an electrode. The other copper wire was soldered by indium to ITO film.

4.1 NiO-ZnO nanorods p-n heterojunctions

We produced heterogeneous p-n junctions on the basis of the ZnO nanorods with n-type conductivity and NiO films with p-type conductivity having sufficiently good rectifying characteristics. Figure 13 shows the *I-V* characteristics of a *p*-type NiO/*n*-type ZnO nanorods heterojunction diode measured in dark and UV (420 nm wavelength) illumination at room temperature. Rectifying *I-V* characteristics were obtained with a forward threshold voltage of ~1.5 V. The diode showed a strong, reversible response to above band gap ultraviolet light, with the UV-induced current being approximately a factor of 2.5 larger than the dark current at a given voltage.

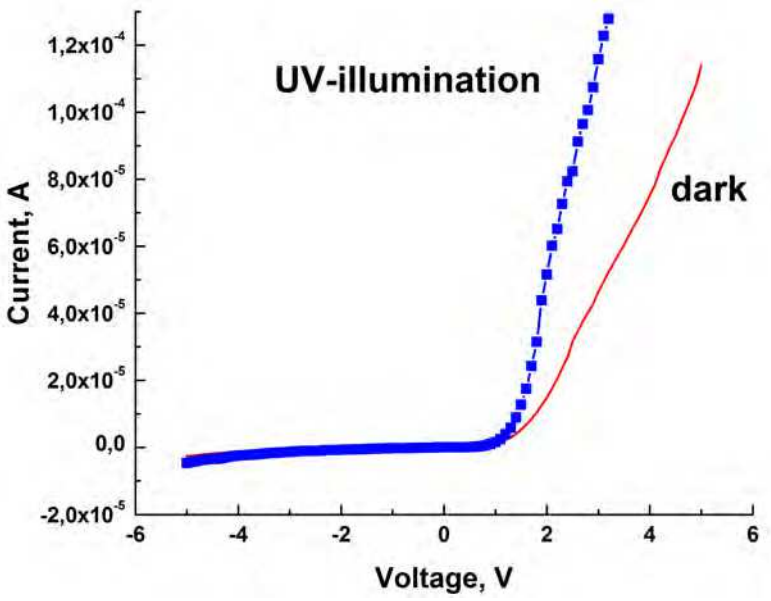

Fig. 13. Typical I-V characteristics of a pn-heterojunction diode under dark and UV-illumination conditions at room temperature. The threshold voltage is ~1.5 V.

Figure 14 (left) shows the *I-V* characteristic of a *n*-type ZnO nanorods/*p*-type NiO heterojunction diode measured in dark. Rectifying *I-V* characteristics were obtained with a forward threshold voltage of ~1.5 V. A structure of the heterojunction was investigated with the use of a focused ion beam system Strata 201 (FEI Company). A cross-section of the ZnO nanorods coated by NiO was prepared by FIB milling. Figure 14 (right) shows FIB image of the cross-section. It is seen in the picture that nickel oxide grown on ZnO nanorods have a fiber structure with fiber diameters of ~50 nm and fiber length of ~100 – 500 nm.

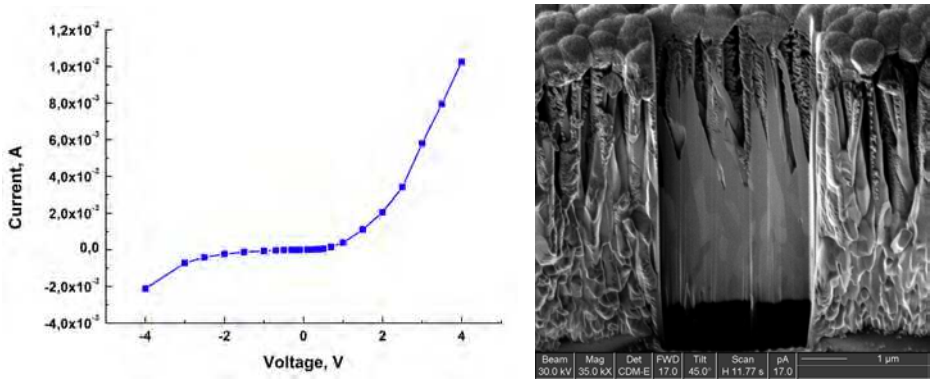

Fig. 14. (Left) Typical I-V characteristics of a pn-heterojunction diode under dark conditions at room temperature. The threshold voltage is ~1.5 V. (Right) FIB image of the cross-section of the ZnO nanorods coated by NiO, prepared by FIB milling.

4.2 Inorganic-organic hybrid diodes

Figure 15 shows the *I-V* characteristics of an inorganic-organic pn-heterojunction diode measured in dark and UV illumination at room temperature. Rectifying *I-V* characteristics were obtained with a forward threshold voltage of ~0.4 V. The inorganic-organic pn-heterojunction diode showed a strong, reversible response to above band gap ultraviolet light, with the UV-induced current being approximately a factor of 10 larger than the dark current at a given voltage in a negative branch and a factor of 1.7 in a positive branch. Electroluminescence was observed in such diodes. The emission has been detected at ~15 V.

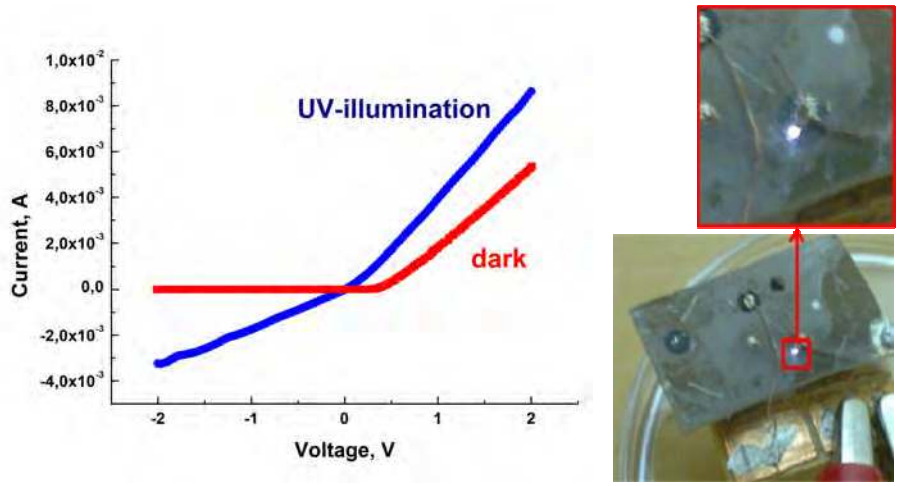

Fig. 15. *I-V* characteristics of the inorganic-organic pn-heterojunction diode under dark and UV-illumination conditions at room temperature (left). The optical micrograph of blue-white emission from the inorganic-organic diode (right).

5. Thermal growth of ZnO nanorods from salt composites

It is well known that the dopants can control the electronic and luminescence properties of the material. In recent years, attention has also focused on spin-dependent phenomena in dilute magnetic zinc oxide in which stoichiometric fraction of the zinc atoms are replaced by transition metal atoms. The growth from the salt mixture is promising method for doping of ZnO nanorods by transition metals and acceptor dopants.

ZnO nanorods were prepared by thermal growth from the solution processed precursor using a freeze drying and milling technique (Baranov et al., 2004). The details of nanorods growth were described earlier (Baranov et al., 2005). Synchrotron X-ray diffraction and high temperature SEM examinations were used to study crystallochemical and morphological evolution of a ZnO-NaCl system during thermal processing.

Aqueous solution of 0.5M $Zn(NO_3)_2$ and $Mn(CH_3COO)_2$ in a Zn/Mn mole ratio of 50/1 (sample Mn2) was vigorously mixed with excessive amount of 2M $(NH_4)_2CO_3$ solution. Aqueous solution for the second sample (MS) was prepared from $Zn(NO_3)_2$ $6H_20$, $Mn(CH_3COO)_2$ $4H_2O$ and $SnCl_2$ $2H_2O$ in a Zn/Mn/Sn mole ratio of 20/1/1. A few drops of

concentrated nitric acid were added to avoid hydrolysis of $SnCl_2$ at dissolution. Then the solution was precipitated by excessive amount of 2M aqueous $(NH_4)_2CO_3$ solution. Precipitates were centrifuged, thoroughly washed by distilled water and freeze dried at P = 5 Pa using Alpha 2-4 (Christ, Germany) laboratory freeze drier. The main component of as-obtained powder samples was zinc carbonate hydroxide $Zn_2(OH)_2CO_3 \bullet xH_2O$ (ZCH) composed of 50 nm diameter amorphous nanofibres. Mixture of the Zn-containing precursor with $NaCl/Li_2CO_3$ salt composition in a 0.5/9/1 weight ratio was milled for 12 h in zirconia jar with zirconia balls using Pulverisette 5 (Fritsch) planetary mill at 700 rpm. Growth of ZnO nanorods was performed from the as-prepared powder in a muffle furnace at 700°C for two hours. Finally product was placed onto dense paper filter and salts were washed many times by water. Supernatant solution was checked on the absence of Cl^- anions by reaction with aqueous solution of $AgNO_3$.

For the synthesis of iron doped nanorods we prepared aqueous solutions of $Zn(NO_3)_2$ and $Fe(NO_3)_3$ salts in a Zn/Fe mole ratio of 100/3 (sample ZnO:FeLi). All other procedures were performed as previously described.

For the synthesis of antimony doped nanorods we dissolved ZnO in a concentrated nitric acid. $SbCl_3$ was added to the hot tartar acid solution and dissolved upon boiling in accordane with reaction:

$$SbCl_3 + 3H_2C_4H_4O_6 \rightarrow Sb(HC_4H_4O_6)_3 + 3HCl\ .$$

Then zinc and antimony contained solutions were mixed in order to obtain 0.01, 0.1, 0.3, 0.5, 0.7, 1 molar % of Sb. All other procedures were performed as previously described.

Elemental analysis was performed by mass-spectrometer Optima 3000XL ICP (Perkin Elmer). For analysis diluted solutions of analyzed samples were prepared (~1 mg of nanorods per 1000 ml of solution in 0.01 M hydrochloric acid). Atomization and ionization were reached by inductive coupled plazma. Calibration was made using standard solutions with known concentration of Sb, Fe, Mn, Li.

SEM (Philips SEM or Supra 50VP (LEO) measurements and cathodoluminescence (CL) spectra of the samples were taken by XL 30S FEG high-resolution scanning electron microscope (HRSEM) with a MonoCL system for CL spectroscopy, and energy dispersive X-ray analysis were used to examine the samples. The morphologies and size distributions of ZnO nanorods were examined by using the JEM-4010 high-resolution transmission electron microscope (HRTEM) at the accelerated voltage of 400kV. TEM with EDAX was employed for characterization of microstructure and distribution of Mn and Sn ions in the ZnO matrix. Magnetic properties of the samples were examined using a Quantum Design SQUID magnetometer in the temperature range from 5 K to 300 K. X-ray powder diffraction (XRD) data of the synthesized nanorods have been collected by a Rigaku D/MAX 2500 (CuK_α.radiation).

Figures 16 (top) and (bottom) show HRSEM images of Mn and MnSn-doped ZnO nanorods, respectively M2 and MS samples, synthesized from the $NaCl\text{-}Li_2CO_3$-containing salt mixture. The detailed SEM analysis revealed that as-prepared ZnO nanorods are straight in morphology and smooth on the surface. Both samples show the quite uniform nanorods with diameters ranging from 15 to 100 nm and from 0.5 to 5 μm in length. The size and the

shape of the nanorods correlate well with the annealing temperature in the range 600-700°C. ZnO nanorods of the smallest size were formed at 600°C. Our experiments have shown that the resulting morphologies strongly depend on the growth temperature.

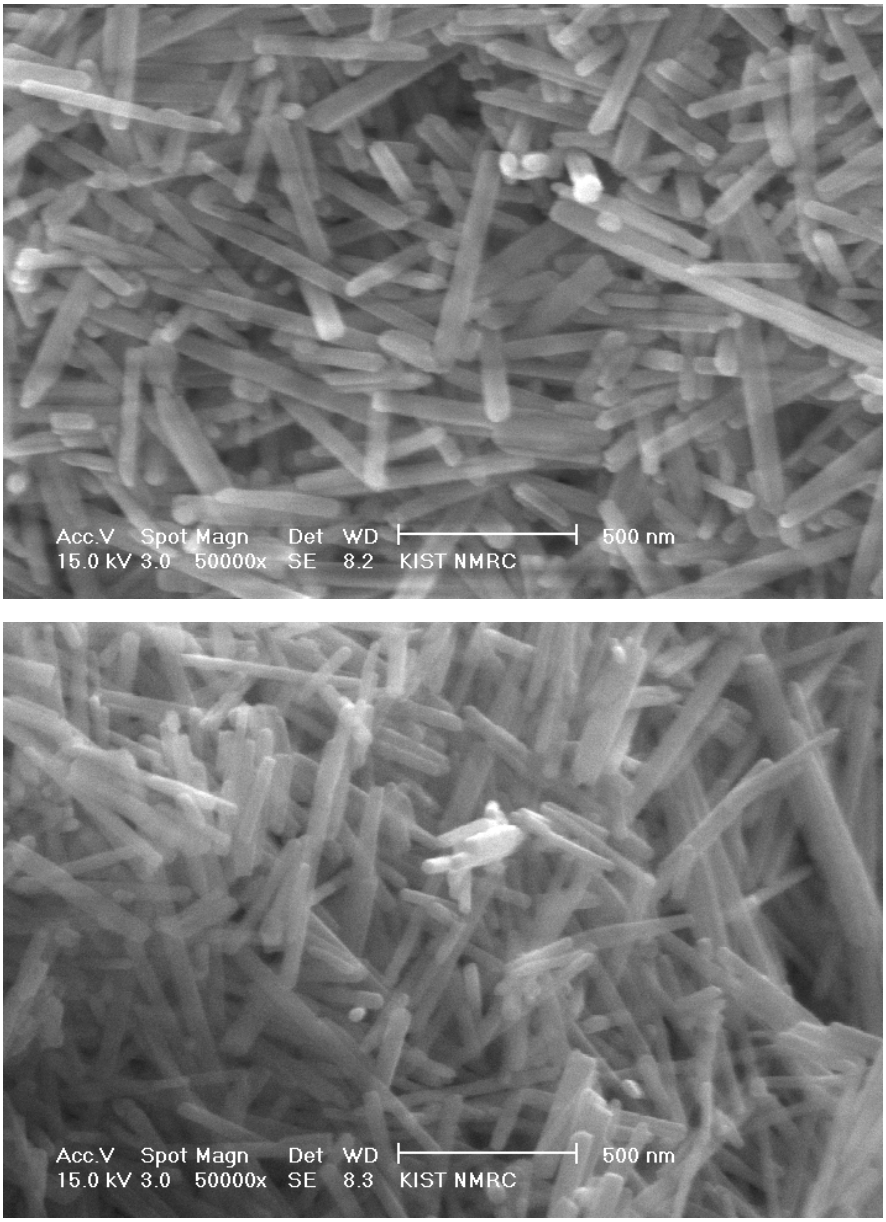

Fig. 16. High resolution scanning electron microscopy images of ZnO nanorods doped with Mn (top) and Mn and Sn (bottom).

Figure 17 shows XRD patterns of Mn (Fig. 17a) and MnSn-doped (Fig. 17b) ZnO nanorods. All the main peaks in Figures 17a and 17b match well with zincite (S.G. P63/mmc (186); JCPDS card 36-1451) although some minor unidentified impurities are obviously present in the samples.

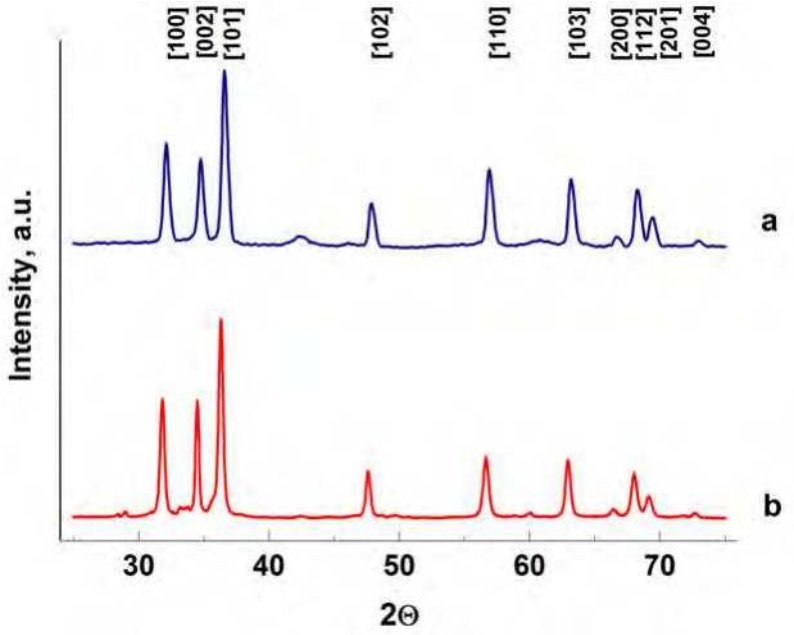

Fig. 17. XRD patterns of ZnO nanorods doped with (a) Mn and (b) Mn and Sn.

The lattice parameters of the samples a = 3.2472(2) Å and c=5.1981(8) (M2 sample), and a = 3.234(2) Å and c= 5.179(4) nm Å (MS sample) were calculated from XRD data. These parameters differ slightly from those of bulk ZnO (a = 3.2498(9) Å and c = 5.20661(15) Å). The lattice parameters for samples M2 and MS revealing that the doping of Mn and Mn/Sn, does not change the wurtzite structure of ZnO, but lead to moderate decreasing of lattice parameters indicating doping effect.

To assess stoichiometry of ZnO nanorods and distribution of Mn and Sn ions in samples, energy dispersive X-ray spectrometry of individual ZnO nanorods was performed using a high-resolution TEM. Manganese and tin contents did not exceed 1 and 0.3 at %, respectively, for the sample marked as MS. For the sample M2 manganese was not more than 0.5%. High-resolution TEM (Fig. 18) confirmed that the nanorods grow along the c-axis direction. Manganese and tin incorporate into the ZnO lattice instead of being precipitated, demonstrated neither second phase inside the nanorods, nor attachments at the nanorod surface. Both the selected area electron diffraction (SAED) pattern and HRTEM images revealed an ordered structure of ZnO hexagonal structure. The absence of any superstructure reflection in the SAED pattern images indicates the absence of any additional long- or short-range ordering in the samples. The typical single crystal defects like twins are obvious from the pictures and denoted by arrows.

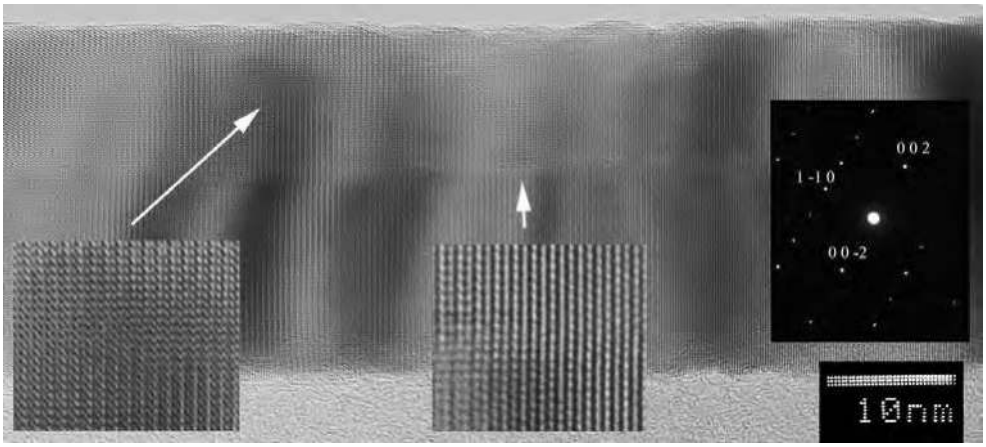

Fig. 18. High resolution transmission electron microscopy images of ZnO nanorods doped with Mn and Sn. Insets: selected area of electron diffraction viewed along [110] direction and the ZnO atom-scale resolution images.

6. Planar device structures from doped ZnO nanorods synthesized by the thermal growth from salt composites

6.1 Resistance switching in ZnO:Fe,Li nanorods

Individual ZnO nanorods doped by Fe, Li were configured as two terminal devices with the Al electrode-ZnO-Al electrode structure on an oxidized silicon substrate (fig.19). E-beam lithography was used to pattern electrodes contacting individual nanowires. Electrical transport properties of the nanorods were studied by applying to the electrodes quasi-dc voltage 0→3→ –3→ 0 with a constant sweep velocity.

The current-voltage characteristics of the ZnO:2%Fe,Li nanorods exhibits a rectifying behavior indicating the Schottky-like barrier formation and displays stable hysteresis (fig.20). The hysteresis at negative voltages is more pronounced than at positive voltages. The nanorod starts in the low resistive state when sweeping the voltage from zero to positive voltages. In the subsequent voltage sweep from positive to negative the nanorod shows an increased resistance. At negative voltage the nanorod resistance switches back from a high to a low resistance. The virgin nanorod shows a higher resistance than obtained in the subsequent cycles with a carrier injection. In contrast to abrupt resistance changes, a smooth resistance change is observed. It is likely, that electric-field domains are built and attenuated resulting in the observable switching effect. Moreover one has to take a nonuniform distribution of trapped charges and the surface band bending into account, which can be altered by applying voltage in forward or reverse directions. Two state resistive switching at RT can be realized using the ZnO nanorods. Emploing a positive voltage of +3V switches the nanorod device into a high impedance state. After applying negative voltage of -3 V the low impedance state is recovered. Between these write and erase voltages the state can be readout with 1.5V (fig.21) (Panin et al., 2007a, 2007b).

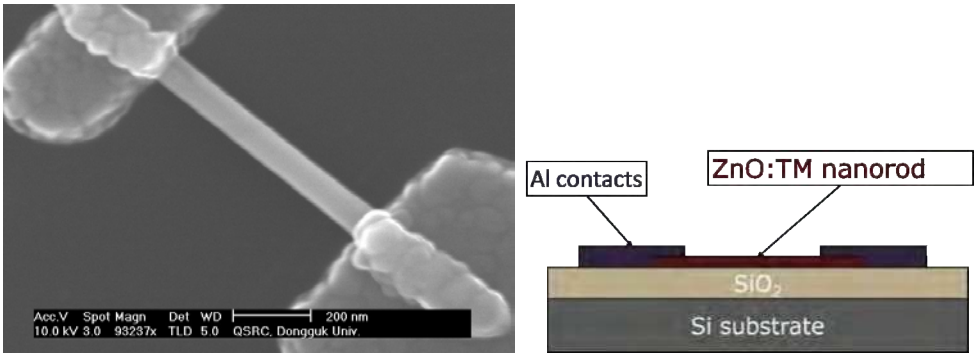

Fig. 19. A SEM image (left) and a scheme (right) of the nanorod with deposited Al contacts patterned by e-beam lithography.

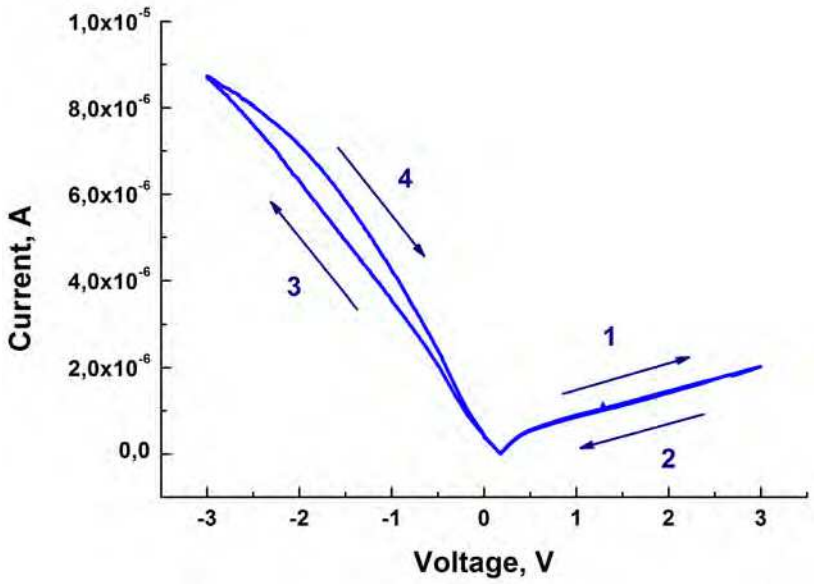

Fig. 20. *I-V* characteristics of a ZnO:2%Fe,Li nanowire for a voltage sweep from 0→3→-3→0 V.

6.2 Field effect transistors from Cr- and Sb-doped ZnO nanorods

Devices for transport measurements were fabricated from Cr- and Sb-doped ZnO nanorods using standard photo- and electron beam lithography and a lift-off technique (Kononenko et al., 2009). Nanorods were transferred onto the surface of thermally oxidized silicon chips with Au pads and lanes. E-beam lithography and a lift-off process were used to pattern e-beam evaporation deposited aluminum electrodes contacting a single nanorods. Two-terminal structures were used for measurements of *I-V* characteristics. n^+ Si(100) substrate is used as a gate. Diameters of both Cr-doped and Sb-doped nanorods were about 50 nm.

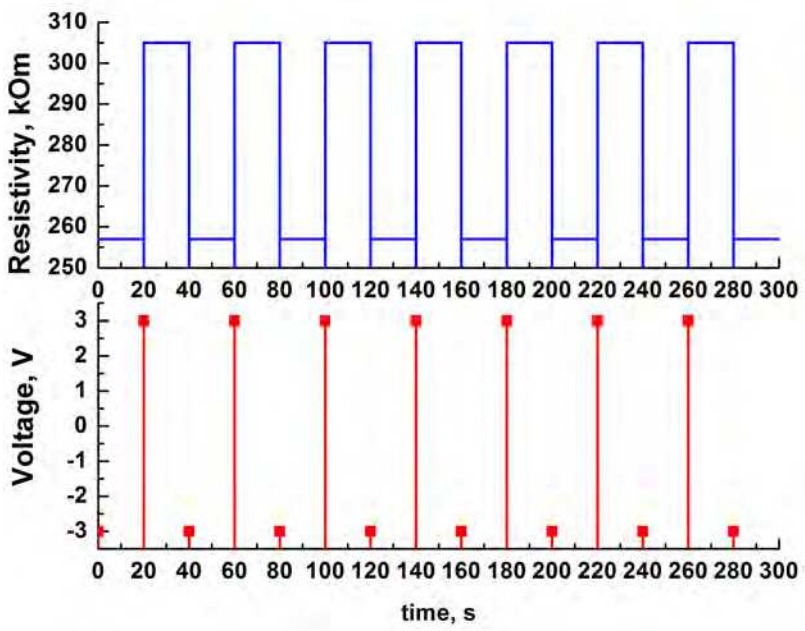

Fig. 21. Two state resistive switching of the ZnO nanowire device at RT. Applied voltage versus time (lower curve); readout resistance versus time (upper curve).

The electrical characteristics of Cr- and Sb-doped ZnO nanorods are shown in figures 22 and 23. The current-voltage curves were measured under different back gate voltages. Conductance of the nanorod increases with increasing back gate voltage which can be explained using energy band bending caused by back gating (Tans et al., 1998). The positive back gate potential increases electron concentration and bends the conduction band towards the Fermi level. Result of that is increasing of conductance. The negative back gate depletes the electron concentration. The conduction band bends from the Fermi level, yielding lower conductance. From the dependence of source-drain current on gate voltages we found that source-drain current increased with changing of voltages from negative to positive in both Cr-doped and Sb-doped nanorods. That is both transistors are n-channel.

We also observed from data of source-drain current versus gate voltages that threshold voltage is about +6V for the Cr-doped nanorods and that is about -7V for the Sb-doped nanorods. It indicates that first one is n-channel enhancement-mode FET and second one is n-channel depletion-mode FET. An on/off current ratio in both FETs as large as 10^5.

It is known that the electronic transport of nanowires can be strongly influenced by the surface effects due to such surface states and/or defects (Dayeh et al., 2007, Jones et al., 2007, Hanrath & Korgel 2005a, Hanrath & Korgel 2005b). Therefore, control of the density of surface states is a key factor in various device applications. Hong et al. have previously reported that ZnO nanowire FETs with n-channel depletion-mode and enhancement-mode transistors can be realized due to the difference of surface states and/or defects induced by the surface morphology of ZnO nanowire side walls (Hong et al., 2007). The realization of

such nanowire transistors having different operational modes can lead to wide applications for the logic circuits (Park et al., 2005).

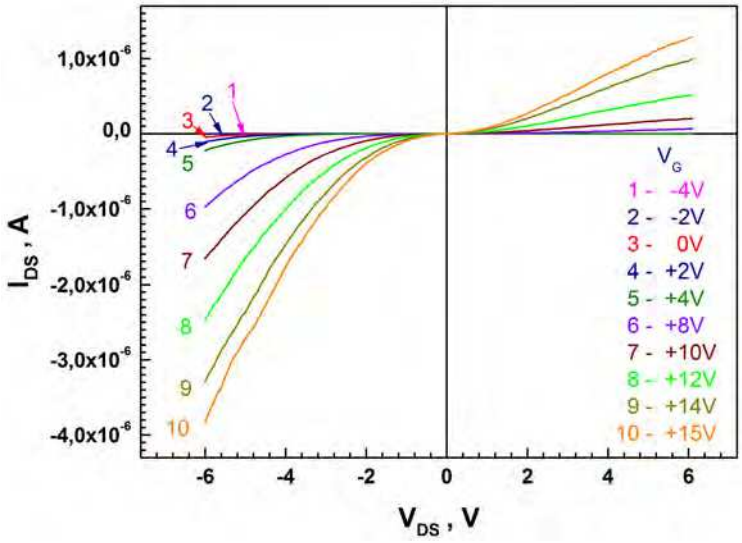

Fig. 22. Output characteristics (I_{DS}-V_{DS}) for Cr-doped nanorod n-channel enhancement-mode FET.

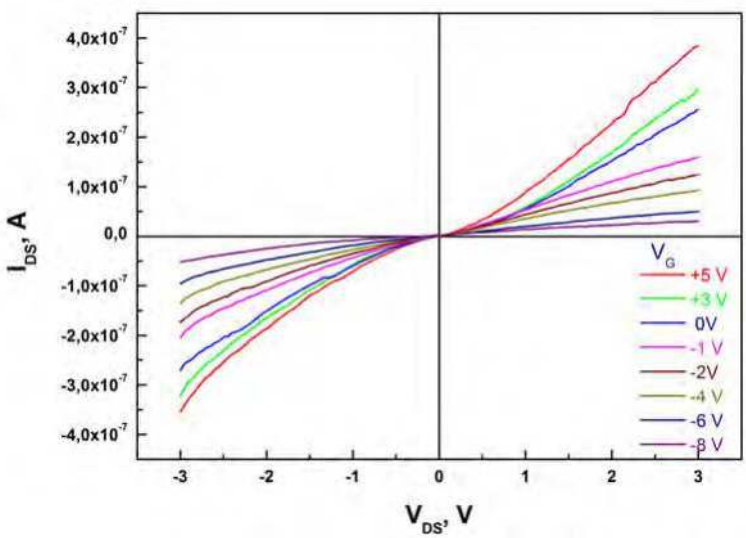

Fig. 23. Output characteristics (I_{DS}-V_{DS}) for Sb-doped nanorod n-channel depletion-mode FET.

The surface depletion can have a significant influence on the electronic transport behavior of ZnO nanorods since the depletion width can be comparable to the diameter size of nanorod.

The trapping of carrier electrons in trap states can cause electron depletion in the channel. The depletion width in small diameter nanorods can be comparable to the diameter size of nanorod. In our case Cr-doped nanorod is completely depleted under the no gate bias condition due to the larger depletion region than the nanorod diameter and Sb-doped nanorod is partially depleted under the no gate bias condition due to the smaller depletion region than the nanorod diameter. Since the diameters of both nanorods are the same, the surface states discrepancy can be connected with dopant concentration or dopant nature. Additional investigations is necessary to clarify this issue.

7. Conclusion

In conclusion, arrays of high crystalline and optical quality ZnO nanorods vertically oriented to a substrate surface can be grown on single-crystalline and amorphous substrates by catalyst-free elemental chemical vapor deposition at a reduced pressure and large excess of zinc vapor. A low level of intrinsic defects in such nanorods facilitates inversion of n-type conductivity to p-type one at doping by acceptor impurity. Homogeneous p-n junctions were formed in vertically aligned ZnO nanorods by diffusion of antimony deposited onto their tops during annealing. Inorganic and inorganic-organic heterogeneous p-n junctions were fabricated on the basis of vertically aligned ZnO nanorods. Blue-white emission was observed from the homogeneous p-n junction ZnO nanorod and inorganic-organic hybrid diodes.

The growth from the salt mixture is promising method for doping of ZnO nanorods by transition metals and acceptor dopants in order to control the electronic and luminescence properties of the nanorods. ZnO nanorods doped by transition metals and acceptor dopants can be used for nanoelectronic applications. Two-level resistive switching of ZnO:Li,Fe nanorods at room temperature were demonstrated. Si back gate Field Effect Transistors were fabricated from Cr- and Sb-doped ZnO nanorods. Transport properties of the Field Effect Transistors were investigated. We found that both type (Cr-doped and Sb-doped) of transistors are n-channel. Field Effect Transistor fabricated from ZnO:Cr nanorod demonstrated enhancement mode behavior and Field Effect Transistor fabricated from ZnO:Sb nanorod demonstrated depletion mode behavior. It can be important for design of ZnO nanorod logic circuits.

8. Acknowledgment

This work was supported by the Russian Ministry of Science and Education grant 02.740.11.5215 and the program of basic research of Presidium of the Russian Academy of Sciences “Foundation of basic research of nanotechnologies and nanomaterials”. The authors would like to thank Dr. A. Irzhak (Common Use Scientific Center of Materials Science, State Technological University "Moscow Institute of Steel and Alloys" (MISIS)) for investigation of specimens in the FIB system, Mr. V.T. Volkov for e-beam deposition of electrode metals.

9. References

Baranov, A.N., Chang, C.H., Shlyakhtin, O.A., Panin, G.N., Kang, T. . & Oh, Y.-J. (2004). In Situ Study of the ZnO–NaCl System During the Growth of ZnO Nanorods. *Nanotechnology,* Vol. 15, No 11, (Nov 2004), PP. (1613-1619), ISSN 0957-4484.

Baranov, A.N., Panin, G.N., Kang, T.W. & Oh, Y.-J. (2005). Growth of ZnO Nanorods from a Salt Mixture. *Nanotechnology* Vol. 16, No. 9, (Sep 2005), PP. (1918-1923), ISSN 0957-4484.

Collins, C.B., Carlson, R.O. & Gallagher, C. (1957). Properties of Gold-Doped Silicon. *Phys. Rev.* Vol. 105, No. 4, (Feb 1957), PP. (1168–1173), ISSN 0031-899X

Dayeh, S.A., Soci, C., Yu, P.K.L., Yu, E. T., Wang, D. (2007). Influence of Surface States on the Extraction of Transport Parameters from InAs Nanowire Field Effect Transistors. *Appl. Phys. Lett.*, Vol.90, No 16, (Apr 2007), PP. (162112-1-162112-3), ISSN 0003-6951.

Fan Z. & Lu, J.G. (2005). Gate-refreshable Nanowire Chemical Sensors. *Appl. Phys. Lett.,* Vol. 86, No. 12, (Mar 2005), PP. (123510-1-123510-3), ISSN 0003-6951.

Govender, K., Boyle, D.S., O'Brien, P., Binks, D., West, D. & Coleman, D. (2002). Room-temperature Lasing Observed from ZnO Nanocolumns Grown by Aqueous Solution Deposition. *Adv. Mater.*, Vol. 14, No. 17, (Sep 2002), PP. (1221–1224), ISSN: 0935-9648.

Gruzintsev, A.N. & Yakimov, E.E. (2005). Annealing Effect on the Luminescent Properties and Native Defects of ZnO. *Inorg. Mater.,* Vol. 41, No. 7, (Jul 2005), PP. (725–729), ISSN: 0020-1685.

Hanrath, T. & Korgel, B.A. (2005). Influence of Surface States on Electron Transport through Intrinsic Ge Nanowires. *J. Phys. Chem. B,* Vol. 109, No. 12, (Mar 2005), PP. (5518-5524), ISSN 1089-5647.

Hu, J.Q., Bando, Y. & Liu, Z.W. (2003). Synthesis of Gallium-Filled Gallium Oxide–Zinc Oxide Composite Coaxial Nanotubes. *Adv. Mater.*, Vol. 15, No. 12, (Jun 2003), PP. (1000-1003), ISSN: 0935-9648.

Hong, W.-K., Hwang, D.-K., Park, I.-K., Jo, G., Song, S., Park, S.-J., Lee, T., Kim, B.-J., Stach, E.A. (2007). Realization of Highly Reproducible ZnO Nanowire Field Effect Transistors With *n*-channel Depletion and Enhancement Modes. *Appl. Phys. Lett.* Vol. 90, No. 24, (Jun 2007), PP. (243103-1-243103-3), ISSN 0003-6951.

Huang, M.H., Mao, S., Feick, H., Yan, H.Q., Wu, Y.Y., Kind, H., Weber, E., Russo, R. & Yang, P.D. (2001). Room-temperature Ultraviolet Nanowire Nanolasers. *Science*, Vol. 292, No. 5523, (Jun 2001), PP. (1897–1899), ISSN 0036-8075.

Jones, F., Léonard, F., Talin, A.A. & Bell, N.S. (2007). Electrical Conduction and Photoluminescence Properties of Solution-grown ZnO Nanowires. *J. Appl. Phys.,* Vol. 102, No. 1, (Jul 2007), PP. (014305-1-014305-7), ISSN 0021-8979.

Kim, S.-W., Fujita, Sh. & Fujita Sh. (2005). ZnO Nanowires with High Aspect Ratios Grown by Metalorganic Chemical Vapor Deposition Using Gold Nanoparticles. *Appl. Phys. Lett.,* Vol. 86, No. 15, (Apr 2005), PP. (153119-1-153119-3), ISSN 0003-6951.

Konenkamp, R., Word, R. C. & Schlegel, C. (2004). Vertical Nanowire Light-emitting Diode. *Appl. Phys. Lett.*, Vol. 85, No. 24, (Dec 2004), PP. (6004-6006), ISSN 0003-6951.

Konenkamp, R., Word, R.C. & Godinez, M. (2005). Ultraviolet Electroluminescence from ZnO/polymer Heterojunction Light-emitting Diodes. *Nano Lett.,* Vol. 5, No. 10, (Oct 2005), PP. (2005–2008), ISSN 1530-6984.

Kononenko, O.V., Redkin, A.N., Panin, G.N., Baranov, A.N., Firsov, A.A., Levashov, V.I., Matveev, V.N. & Vdovin, E.E. (2009). Study of Optical, Electrical and Magnetic Properties of Composite Nanomaterials on the Basis of Broadband Oxide Semiconductors. *Nanotechnologies in Russia,* Vol. 4, Nos. 11–12, (Apr 2009), PP. (822–827), ISSN 1995-0780.

Krumeich, F., Muhr, H. J., Niederberger, M., Bieri, F., Schnyder, B. & Nesper, R. Morphology and Topochemical Reactions of Novel Vanadium Oxide Nanotubes. (1999). *J. Am. Chem. Soc.,* Vol. 121, No. 36, (Sep 1999), PP. (8324-8331), ISSN 0002-7863.

Law, M., Greene, L.E., Johnson, J.C., Saykally, R. & Yang, P.D. (2005). Nanowire Dye-sensitized Solar Cells. *Nat. Mater.*, Vol. 4, No. 6, (Jun 2005), PP. (455–459), ISSN 1476-1122.

Lee, Y.-J., Sounart, T.L., Scrymgeour, D.A., Voigt, J.A. & Hsu, J.W.P. (2007). Control of ZnO Nanorod Array Alignment Synthesized Via Seeded Solution Growth. *Journal of Crystal Growth,* Vol. 304, No. 1, (Jun 2007), PP. (80–85), ISSN 0022-0248.

Liu, F., Cao, P.J., Zhang, H.R., Shen, C.M., Wang, Z., Li, J.Q. & Gao, H.J. (2005). Well-aligned Zinc Oxide Nanorods and Nanowires Prepared Without Catalyst. *Journal of Crystal Growth,* Vol. 274, No. 1-2, (Jan 2005), PP. (126–131), ISSN 0022-0248.

Look, D.C., Claflin, B., Alivov, Y.I. & Park, S.J. (2004). The Future of ZnO Light Emitters. *Phys. Status Solidi A,* Vol. 201, No.10, (Aug 2004), PP. (2203–2212), ISSN 1862-6300.

Oh, S.H., van Benthem, K., Molina, S.I., Borisevich, A.Y., Luo, W., Werner, P., Zakharov, N.D., Kumar, D., Pantelides, S.T. & Pennycook, S.J. (2008). Point Defect Configurations of Supersaturated Au Atoms Inside Si Nanowires. *Nano Lett.,* Vol. 8, No. 4, (Apr 2008), PP. (1016–1019), ISSN 1530-6984.

Ohta H. & Hosono H. (2004). Transparent Oxide Optoelectronics, *Mater. Today,* Vol. 7, No. 6, (Jul 2004), PP. (42-51), ISSN 1369-7021.

Özgür, Ü., Alivov, Ya.I., Liu, C., Teke, A., Reshchikov, M.A., Doğan, S., Avrutin, V., Cho, S.-J. & Morkoç H.J. (2005). A Comprehensive Review of ZnO Materials and Devices. *J. Appl. Phys.*, Vol. 98, No. 4, (Aug 2005), PP. (041301-1-041301-103), ISSN 0021-8979.

Park, J., Choi, H.-H., Siebein, K. & Singh, R.K. (2003). Two-Step Evaporation Process for Formation of Aligned Zinc Oxide Nanowires. *J. Cryst. Growth,* Vol. 258, No.3–4, (Nov 2003), PP. (342–348), ISSN 0022-0248.

Park, W.I., Yi, G.-C., Kim, M.Y. & Pennycook, S.J. (2003). Quantum Confinement Observed in ZnO/ZnMgO Nanorod Heterostructures. *Adv. Mater.,* Vol. 15, (Mar 2003), No. 6, PP. (526-529), ISSN 0935-9648.

Park, W.I. & Yi, G. C. (2004). Electroluminescence in *n*-ZnO Nanorod Arrays Vertically Grown on *p*-GaN. *Adv. Mater.,* Vol. 16, No. 1, (Jan 2004), PP. (87-90), ISSN 0935-9648.

Park, W.I., Kim, J.S., Yi, G.-C. & Lee, Y.-J. (2005). ZnO Nanorod Logic Circuits. *Adv. Mater.,* Vol. 17, No. 11, (Jun 2005), PP. (1393-1397), ISSN 0935-9648.

Panin, G., Baranov, A.N., Kang, T.W., Kononenko, O.V., Dubonos, S.V., Min, S. K., and Kim H. J. (2007a). Electrical and Magnetic Properties of Doped ZnO Nanowires. *Mater. Res. Soc. Symp. Proc.* Vol. 957, PP. (0957-K04-06-1-0957-K04-06-6), ISBN 9781558999145, San Francisco, California, USA, April 9-13, 2007.

Panin, G., Baranov, A.N., Kononenko, O.V., Dubonos, S.V., and Kang, T.W. (2007b). Resistance Switching Induced by an Electric Field in ZnO:Li, Fe Nanowires. *AIP Conf. Proc.,* Vol. 893, PP. (743-744), ISBN: 978-0-7354-0397-0, Vienna, Austria, July 24-28, 2006.

Red'kin A.N., Makovei Z.I., Gruzintsev A.N., Dubonos S.V. & Yakimov E.E. (2007). Vapor Phase Synthesis of Aligned ZnO Nanorod Arrays from Elements. *Inorganic Materials,* Vol. 43, No. 3, (Mar 2007), PP. (253–257), ISSN 0020-1685.

Red'kin, A., Makovei, Z., Gruzintsev, A., Yakimov, E., Kononenko, O.V. & Firsov A.A. (2009). Elemental Vapor-Phase Synthesis of Nanostructured Zinc Oxide. *Inorg. Mat.*, Vol. 45, No. 11, (Nov 2009), PP. (1330−1336), ISSN 0020-1685.

Reiser, A., Ladenburger, A., Prinz, G.M., Schirra, M., Feneberg, M., Langlois, A., Enchelmaier, R., Li, Y., Sauer, R. & Thonke, K. (2007). Controlled Catalytic Growth and Characterization of Zinc Oxide Nanopillars on *a*-plane Sapphire. *J. Appl. Phys.*, Vol. 101, No. 5, (Mar 2007), PP. (054319-1-054319-9), ISSN 0021-8979.

Sun, X.W., Huang, J.Z., Wang, J.X. & Xu, Z. (2008). A ZnO Nanorod Inorganic/Organic Heterostructure Light-Emitting Diode Emitting at 342 nm. *Nano Lett.*, Vol. 8, No. 4, (Apr 2008), PP. (1219-1223), ISSN 1530-6984.

Tans, S.J., Verschueren, A.R. M. & Dekker C. (1998). Room-temperature transistor based on a single carbon nanotube. *Nature,* Vol. 393, No. 6680, (May 1998), PP. (49-52), ISSN 0028-0836.

Umar, A., Kim, S.H., Lee, Y.-S., Nahm, K.S. & Hahn, Y.B. (2005). Catalyst-free Large-quantity Synthesis of ZnO Nanorods by a Vapor–solid Growth Mechanism: Structural and Optical Properties. *Journal of Crystal Growth,* Vol. 282, No. 1-2, (Aug 2005), PP. (131–136), ISSN 0022-0248.

Wang, R. C., Liu, C. P., Huang, J. L. & Chen, S.-J. (2005). ZnO Hexagonal Arrays of Nanowires Grown on Nanorods. *Appl. Phys. Lett.,* Vol. 86, No. 25, (Jun 2005), PP. (251104-1-251104-3), ISSN 0003-6951.

Wei, M., Zhi, D. & MacManus-Driscoll, J.L. (2005). Self-catalysed Growth of Zinc Oxide Nanowires. *Nanotechnology,* Vol. 16, No. 8, (Aug 2005), PP. (1364–1368), ISSN 0957-4484.

Wei, Y.G., Xu, C., Xu, S., Li, C., Wu, W.Z. & Wang, Z.L. (2010). Planar Waveguide-nanowire Integrated Three-dimensional Dyesensitized Solar Cells. *Nano Lett.*, Vol. 10, No. 6, (Jun 2010), PP. (2092–2096), ISSN 1530-6984.

Yang, K., She, G.-W., Wang, H., Ou, X.-M., Zhang, X.-H., Lee, C.-S. & Lee, S.-T. (2009) ZnO Nanotube Arrays as Biosensors for Glucose. *J. Phys. Chem. C*, Vol. 113, No. 47, (Nov 2009), PP. (20169 – 20172), ISSN 1932-7447.

Yeh, P.-H., Li, Z. & Wang, Zh.L. (2009). Schottky-Gated Probe-Free ZnO Nanowire Biosensor. *Adv. Mater.,* Vol. 21, No. 48, (Dec 2009), PP. (4975-4978), ISSN 0935-9648.

Zhao, Q.X., Willander, M., Morjan, R.R., Hu, Q.H., Campbell, E.E.B. (2003). *Appl. Phys. Lett.* Vol. 83, No. 1, (Jul 2003), PP. (165-167), ISSN 0003-6951.

Zha, M., Calestani, D., Zappettini, A., Mosca, R., Mazzera, M., Lazzarini, L. & Zanotti, L. (2008). Large-area Self-catalysed and Selective Growth of ZnO Nanowires. *Nanotechnology,* Vol. 19, No. 32, (Aug 2008), PP. (325603-1-325603-5), ISSN 0957-4484.

Zhang, X.-M., Lu, M.-Y., Zhang, Y., Chen, L.-J. & Wang, Zh.L. (2009). Fabrication of a High-Brightness Blue-Light-Emitting Diode Using a ZnO-Nanowire Array Grown on p-GaN Thin Film. *Adv. Mater.,* Vol. 21, No. 27, (Jul 2009), PP. (2767-2770), ISSN 0935-9648.

Zhao, D., Andreazza, C., Andreazza, P., Ma, J., Liu, Y. & Shen, D. (2005). Buffer layer effect on ZnO nanorods growth alignment. *Chemical Physics Letters,* Vol. 408, No. 4-6, (Jun 2005), PP. (335-338), ISSN 0009-2614.

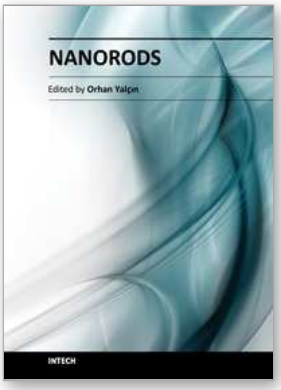

Nanorods

Edited by Dr. Orhan Yalçın

ISBN 978-953-51-0209-0
Hard cover, 250 pages
Publisher InTech
Published online 09, March, 2012
Published in print edition March, 2012

The book "Nanorods" is an overview of the fundamentals and applications of nanosciences and nanotechnologies. The methods described in this book are very powerful and have practical applications in the subjects of nanorods. The potential applications of nanorods are very attractive for bio-sensor, magneto-electronic, plasmonic state, nano-transistor, data storage media, etc. This book is of interest to both fundamental research such as the one conducted in Physics, Chemistry, Biology, Material Science, Medicine etc., and also to practicing scientists, students, researchers in applied material sciences and engineers.

How to reference

In order to correctly reference this scholarly work, feel free to copy and paste the following:

Oleg V. Kononenko, Arkady N. Redkin, Andrey N. Baranov, Gennady N. Panin, Artem A. Kovalenko and Anatoly A. Firsov (2012). ZnO Nanorods: Synthesis by Catalyst-Free CVD and Thermal Growth from Salt Composites and Application to Nanodevices, Nanorods, Dr. Orhan Yalçın (Ed.), ISBN: 978-953-51-0209-0, InTech, Available from: http://www.intechopen.com/books/nanorods/zno-nanorods-synthesis-by-catalyst-free-cvd-and-thermal-growth-from-salt-composites-and-application-

INTECH
open science | open minds

InTech Europe
University Campus STeP Ri
Slavka Krautzeka 83/A
51000 Rijeka, Croatia
Phone: +385 (51) 770 447
Fax: +385 (51) 686 166
www.intechopen.com

InTech China
Unit 405, Office Block, Hotel Equatorial Shanghai
No.65, Yan An Road (West), Shanghai, 200040, China
中国上海市延安西路65号上海国际贵都大饭店办公楼405单元
Phone: +86-21-62489820
Fax: +86-21-62489821